Materials Science & Engineering A 682 (2017) 501–508

Contents lists available at ScienceDirect

Materials Science & Engineering A

journal homepage: www.elsevier.com/locate/msea

Microstructure and mechanical properties of ultrafine-grained aluminum consolidated by high-pressure torsion

Mohammad Khajouei-Nezhad[a], Mohammad Hossein Paydar[a,*], Ramin Ebrahimi[a], Péter Jenei[b], Péter Nagy[b], Jenő Gubicza[b]

[a] Department of Materials Science and Engineering, School of Engineering, Shiraz University, Iran
[b] Department of Materials Physics, Eötvös Loránd University, P.O.B. 32, Budapest H-1518, Hungary

ARTICLE INFO

Keywords:
High-pressure torsion (HPT)
Consolidation
Aluminum
Dislocations
Strength
Ductility

ABSTRACT

Coarse-grained aluminum powder with 99.5 wt% purity was consolidated by high-pressure torsion (HPT) technique at room temperature using a low carbon steel powder holder. In this process, the powder experiences a semi-constrained condition because the internal wall of the powder holder can expand under the load applied during HPT. After 4 turns of HPT a relative density of 99.83% was achieved. The microstructure was characterized by electron backscatter diffraction and X-ray line profile analysis. It was found that the grain size decreased while the dislocation density increased with both increasing the distance from the disk center and the number of HPT turns. The smallest grain size and the maximum dislocation density with the values of 0.41 μm and 6.8×10^{14} m^{-2}, respectively, were achieved at the periphery of the disks processed for 4 turns. Tensile tests showed that the consolidation of this Al powder by 4 turns of HPT yielded a high ultimate tensile strength and a good ductility (~373 MPa and ~22%, respectively). It turned out that the yield strength versus grain size relationship obeys the Hall-Petch equation. This study demonstrates the capability of HPT technique for processing consolidated Al powder with high strength and good ductility.

1. Introduction

Severe plastic deformation (SPD) techniques are generally known as effective methods for improving mechanical properties of materials [1–4]. High-pressure torsion (HPT) is one of the most frequently used SPD methods since its application yields a very high degree of grain refinement in bulk metallic materials [5–9]. In addition to processing of ultrafine-grained (UFG) and nanocrystalline microstructures in bulk coarse-grained materials, HPT technique is also capable of consolidation of metallic [10–13] and ceramic [14–16] powders, as well as their composites [17–19]. Based on the classical HPT technique, numerous new SPD methods were developed, such as high-pressure double-torsion [20–22] or ring-constraint HPT [23]. Jahedi et al. [20] showed that unconstrained HPT and high pressure double torsion processes with hollow holder can be successfully used for consolidation of metallic powders. If the initial powder is coarse-grained, both consolidation and grain refinement occur during HPT. Simulations of constrained, semi-constrained and unconstrained HPT processes revealed that under unconstrained conditions the imposed strain is higher while the temperature rise is less than for other methods, which can facilitate grain fragmentation during HPT [24].

Consolidation of aluminum powders by different SPD methods was extensively studied in the literature [25–33]. Some works reported full densification and superior mechanical properties owing to the high shear strains applied during SPD-processing [25–29]. SPD methods usually lead to fracturing of the native alumina or aluminum hydroxide layer on the surface of aluminum powder particles. Then, these fine secondary phase dispersoids are distributed in the consolidated aluminum matrix and yield excellent mechanical strength and thermal stability of the UFG microstructure [27,29–33]. This effect becomes more significant if the initial powder contains fine particles, since in this case the fraction of native surface phases is relatively large. It is noted that these surface phases may be either crystalline or amorphous. Numerous investigations focused on HPT-processing of pure aluminum powder and aluminum matrix composites [32,34–37], and large strength, good ductility as well as high microhardness values were obtained for pure aluminum powders consolidated at room temperature.

In the present work, a coarse-grained pure aluminum powder is consolidated in a hollow low carbon steel powder holder using HPT technique at room temperature. The microstructures of the aluminum samples consolidated by different turns of HPT are investigated by X-

* Corresponding author.
E-mail address: paaydar@shirazu.ac.ir (M.H. Paydar).

http://dx.doi.org/10.1016/j.msea.2016.11.076
Received 31 July 2016; Received in revised form 19 November 2016; Accepted 22 November 2016
Available online 23 November 2016

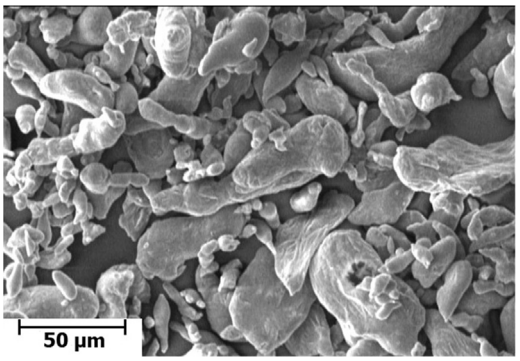

Fig. 1. SEM image of the commercially pure aluminum powder used in this study.

ray line profile analysis (XLPA) and electron backscatter diffraction (EBSD). The crystallite size, the dislocation density and the grain size are determined as a function of distance from the disk center and the number of turns. For the present Al consolidated by HPT, the crystallite size obtained by XLPA is much smaller than the grain size determined by EBSD as the former quantity corresponds rather to the subgrain size. The mechanical properties of the samples are studied by Vickers microhardness and tensile testing, and the yield strength is correlated to the grain size.

2. Experimental material and procedures

2.1. Material processing

The initial material was a commercially pure aluminum powder with irregular particle shape and particle sizes were between 5 and 40 µm. Fig. 1 shows a representative scanning electron microscopy (SEM) image taken on the initial aluminum powder. The chemical composition of the initial powder was measured by optical emission spectroscopy (OES) using a Spectrotest device and shown in Table 1. According to OES analysis, the initial powder is of 2N5 purity. To consolidate the powder by HPT method, a hollow low carbon steel (type: Ck 22) cylinder with two end caps were used as a powder holder. The diameter and the height of the interior of the holder were ~20 mm and ~5 mm, respectively. Fig. 2 shows schematically the steps of powder filling into the hollow low carbon steel holder. The filled holder was placed between two anvils and the HPT process was performed under unconstrained condition. The applied force was ~600 kN, which corresponds to a pressure of ~1.2 GPa and the rotation speed of the bottom anvil was ~0.2 rpm. HPT processing was carried out at room temperature for three different numbers of turns: N=1, 2 and 4. It should be noted, that during consolidation the powder experiences a semi-constrained condition because the internal wall of powder holder expands under the load applied during HPT. Hence, although the hollow powder holder undergoes unconstrained HPT process, the holder wall prevents an intense radial outflow of the softer aluminum material during HPT. It should be noted, however, that the radial expansion of the holder caps was smaller than that for the cylindrical wall, therefore a small fraction of material flowed axially along the holder wall. These ring-shaped parts at the edge of the HPT-processed disks were removed before further investigations. It is also noted that the holder wall serves similarly as the ring in the recently developed ring-constraint HPT [23], i.e., it produces back pressure. This back pressure promotes the consolidation of the powder in the holder. With increasing number of HPT turns, the diameter of the disks increased while the thickness was reduced. The diameter and the thickness of the sample processed by 4 turns of HPT were 22.31 mm and 1.12 mm, respectively.

Table 1
Chemical composition of the initial aluminum powder as determined by OES method (in wt%).

Other elements	Cu	Si	Fe	Al
0.078%	0.047%	0.131%	0.244%	99.5%

2.2. Methods for the investigation of mechanical performance

The Vickers microhardness of the consolidated samples was measured as a function of the position in both radial and axial directions on the cross sections of the HPT-processed disks. The spacing between the neighboring indents in these two-dimensional hardness maps was ~0.3 mm. The surface of the cross section was first mechanically polished using a 3000-grit abrasive paper and then electropolished to a mirror-like quality using a solution of 20 vol% perchloric acid and 80 vol% ethanol with the applied current of 10 A at 0 °C. The load and the dwell time applied in hardness measurements were 100 g and 15 s, respectively.

For tensile testing, dog bone shaped samples were cut by electric discharge machining (EDM), as depicted in Fig. 3. Two samples were fabricated from each disk. As the different numbers of HPT turns yielded different disk thickness values, the specimens cut from the disks were thinned to the same thickness of ~0.9 mm by mechanical polishing. The uniaxial tensile tests were carried out at a strain rate of $\sim 3\times10^{-3}\ s^{-1}$ and room temperature using Santam STM-150 machine.

2.3. Determination of the relative density

The density of the consolidated samples was measured using Archimedes' principle. The mass of the disks was measured using a Sartorius electronic balance (model ED224S) equipped with density determination kit by emerging samples in the distilled water. The precision of the balance was 0.0001 g which yielded an uncertainty of 0.001 g/cm^3 for the measured density. For determining the relative density, the measured density was normalized by the theoretical density of pure aluminum (2.710 g/cm^3). As a consequence, the uncertainty of the relative density was about 4×10^{-4}. For each number of turns, the densities of two HPT disks were determined and their arithmetic average is reported in Table 2. The error was determined as the deviation of the individual relative densities from the average value.

2.4. Procedures for studying the microstructure

The microstructures of the consolidated samples were investigated by EBSD using a FEI Quanta 3D dual beam SEM, equipped with an EDAX type EBSD system and an OIM Analysis 5.3 software. The EBSD studies were carried out along the middle-line on the disk cross-section for three different distance values from the disk center (r): r=0 mm, r=4 mm and r=8 mm. These three locations will be referred to as center, half-radius and periphery in this study. Fig. 3 indicates these locations by black rectangles. The microstructures at the same locations were also studied by XLPA. For both EBSD and XLPA measurements, the specimens were first mechanically polished by a 2500-grit SiC paper and then by an ALOX suspension with a particle size of 1 µm. Finally, the samples were electropolished in an A2 electrolytic solution (made by Struers) at room temperature and a fixed voltage of 10 V for 30 s. The X-ray line profiles were measured by a high-resolution rotating anode diffractometer (type: RA-MultiMax9, manufacturer: Rigaku) using $CuK\alpha_1$ (λ=0.15406 nm) radiation. Two-dimensional imaging plates detected the Debye-Scherrer diffraction rings. The line profiles were determined as the intensity distribution perpendicular to the rings obtained by integrating the two dimensional intensity distribution along the rings.

The X-ray diffraction line profiles were evaluated by the Convolutional Multiple Whole Profile (CMWP) fitting analysis [38]. In this method, the whole measured powder diffraction pattern is fitted

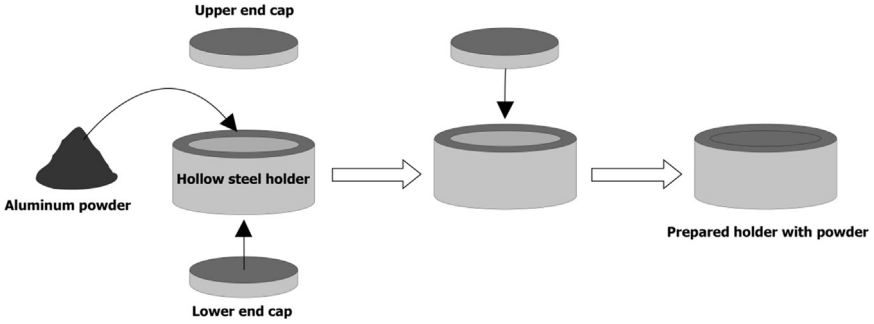

Fig. 2. The steps of aluminum powder filling into the hollow low carbon steel holder.

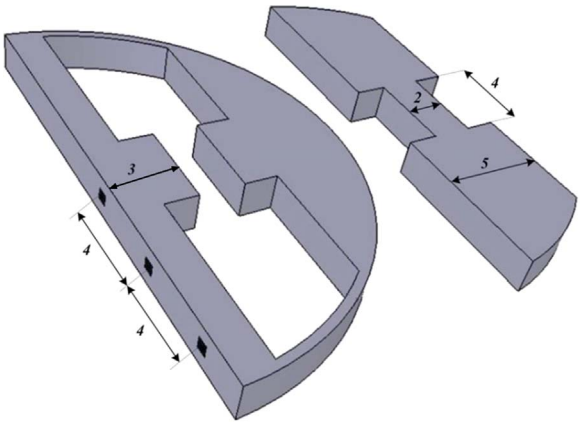

Fig. 3. Schematic showing the dimensions of the miniature tensile specimen (in millimeter) prepared from one-half of HPT-processed disks. The locations of EBSD and XLPA measurements on the cross section of the disk are indicated by black squares.

Table 2
The relative densities for the disks consolidated by HPT.

Sample	Relative density [%]
N=1	99.43 ± 0.14
N=2	99.74 ± 0.11
N=4	99.83 ± 0.09

by a theoretical pattern (I_{fit}) which is calculated as the sum of a background function and calculated theoretical peak profiles:

$$I_{fit}(2\theta) = BG(2\theta) + \sum_{hkl} I_{hkl}^{\max} I_{hkl}(2\theta - 2\theta_B^{hkl}), \quad (1)$$

where $BG(2\theta)$ represents the background, $I_{hkl}^{\max}$ and $2\theta_B^{hkl}$ are the maximum intensity and the position of peak *hkl* in 2θ, respectively. I_{hkl} is the theoretical profile for reflection *hkl* which is obtained as the convolution of the measured instrumental peak (I_{hkl}^{I}) and theoretical profile functions calculated for the broadening caused by crystallite size (I_{hkl}^{S}), dislocations (I_{hkl}^{D}) and planar faults (I_{hkl}^{F}):

$$I_{hkl} = I_{hkl}^{I} * I_{hkl}^{S} * I_{hkl}^{D} * I_{\{hkl\}}^{F}, \quad (2)$$

where the symbol „*" denotes the operation of convolution. The notation {*hkl*} in the subscript of the intensity profile for planar faults indicates that this function is a weighted sum of subreflections related to the same {*hkl*} reflecting plane family. The instrumental pattern was measured on a LaB_6 line profile standard material. The CMWP evaluation program selects automatically the nearest instrumental profile to each diffraction peak of the sample. For the determination of function $BG(2\theta)$ first some base points of the background on the experimental pattern should be specified, and then the background function is determined as the interpolated cubic spline corresponding to the given base points. As the maximum intensity, $I_{hkl}^{\max}$, and the peak position, $2\theta_B^{hkl}$, are independent of the line profile shape, they are treated simply as free fitting parameters and their relation to the microstructure is not investigated in the CMWP procedure. In the calculation of the theoretical profile functions it is assumed that the crystallites have spherical shape with lognormal size distribution and the strain is caused by dislocations. The mathematical form of the theoretical intensity functions related to the crystallite size and the dislocations are given in Ref [38].

The area-weighted mean crystallite size, the dislocation density and the twin-fault probability were evaluated by the CMWP method, where the twin-fault probability is defined as the fraction of twin faults among the {111} lattice planes. The area-weighted mean crystallite size ($< x >_{\text{area}}$) was calculated from the median (m) and the lognormal variance (σ^2) of the crystallite size distribution as:

$$< x >_{area} = m \cdot exp(2.5\sigma^2). \quad (3)$$

3. Results

3.1. Density and microstructure of aluminum samples consolidated by HPT

The average relative density values for the aluminum samples consolidated by HPT are shown in Table 2. A high relative density (99.43%) was obtained even after the first turn of HPT, which only slightly increased with increasing the number of HPT revolutions. After 4 turns of HPT a relative density of 99.83% was achieved.

Fig. 4 shows the EBSD orientation maps obtained for the samples consolidated by N=1 and 4 revolutions. The sample processed by 2 turns is not shown in Fig. 4, as it is very similar to sample N=4. As the torsional strain varies along the disk radius, the microstructure was investigated in the center, half-radius and periphery of the disks for N=1, 2 and 4 turns. The step sizes are about 250 times smaller than the linear dimensions of the images. Therefore, the EBSD step sizes in the images with the lowest and highest magnifications are 150 and 30 nm, respectively. It is noted that the scales in the images taken at the center, half-radius and periphery are different. Fig. 4 shows that the grains are slightly elongated in the radial direction of the HPT-processed disks (horizontal direction in the figure). The area-weighted average grain size was determined from the EBSD images as the average of the equivalent circle diameters weighted by their areas. The average grain size values are listed in Table 3 and plotted in Fig. 5. After 1 turn of HPT, the grain sizes were ~3.3 μm and ~0.63 μm in the center and the periphery of the disk, respectively. Fig. 5 shows that the grain size decreases with increasing the distance from the center for all HPT-processed disks (N=1, 2 and 4). The grain size also decreases with increasing the number of HPT turns, however it saturates at N=2 and no further grain refinement was observed between 2 and 4 revolutions. In this saturated state, the grain size in the center of the disk is still larger than at the periphery due to the much smaller shear strain in the disk center. The smallest achievable grain sizes at the center and

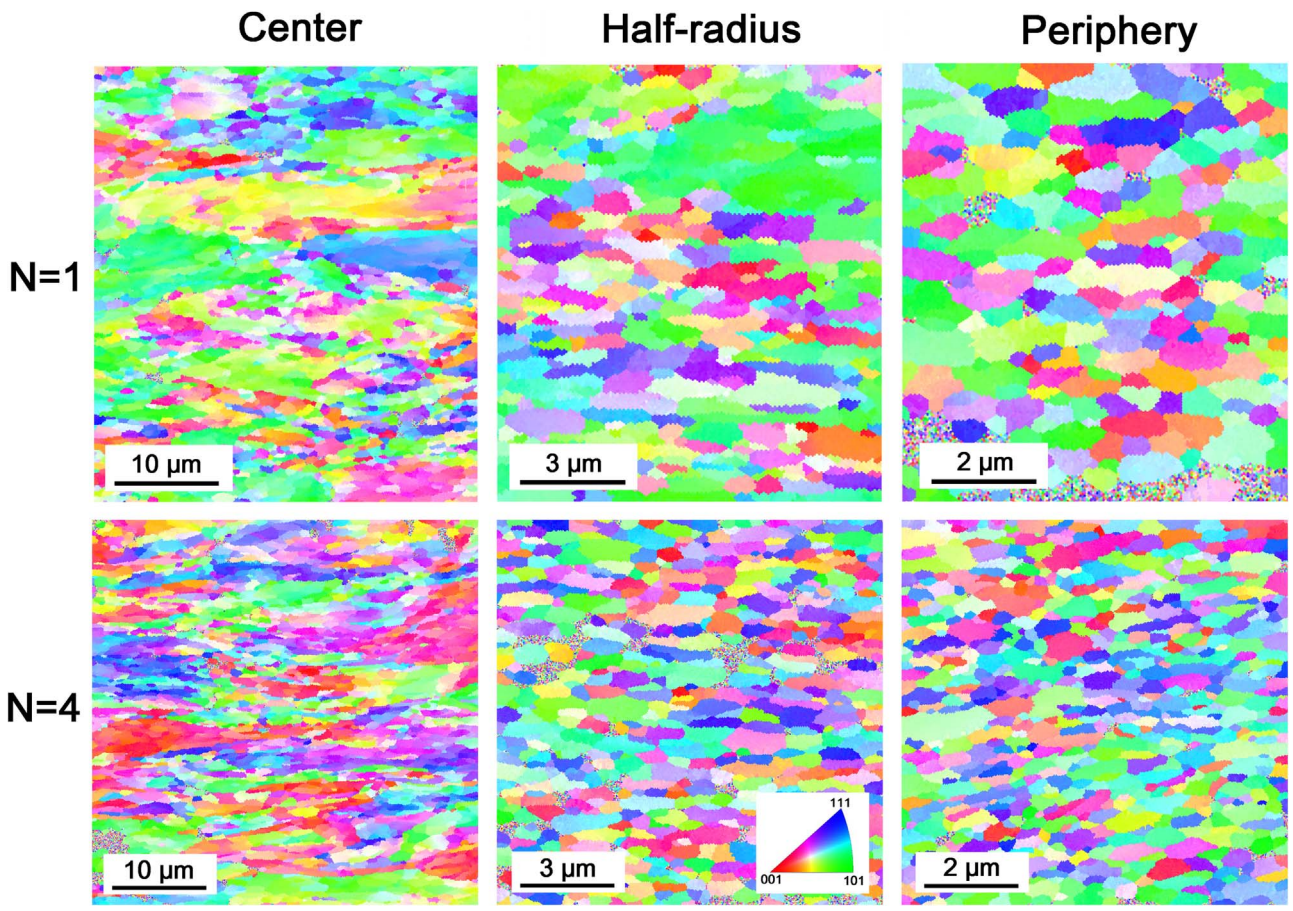

Fig. 4. EBSD images taken on the cross sections of the aluminum disks consolidated by different numbers of HPT turns. For N=1 and 4 the microstructure was investigated in the center, half-radius and periphery. It is noted that the scales in the images taken at the center, half-radius and periphery are different.

periphery obtained after 4 turns were ~1.86 and ~0.41 μm, respectively.

In addition to the grain size, the fractions of low-angle grain boundaries (LAGBs with misorientation angles between 2 and 15°) and high-angle grain boundaries (HAGBs with misorientation angles higher than 15°) were also determined and listed in Table 3. The lowest value of HAGB fraction (~36%) was measured in the center of the sample processed by 1 turn. At the half-radius of this disk the fraction of HAGBs is significantly larger due to the larger imposed strain (54–55%). Considerable difference between the HAGB fractions determined at the half-radius and the periphery was not observed. Similar trend along the disk radius was observed for N=2 and 4. The highest fraction of HAGBs was achieved at the periphery of the disk processed by 4 revolutions (~73%). Fig. 6a and b illustrate the spatial distribution of grain boundaries with different misorientations at the half-radius of the disks processed by 1 and 2 HPT turns, respectively. In these two combined image quality (IQ) and grain boundary maps, red, green and blue colors indicate misorientations in the ranges of 2–5°, 5–15° and 15–60°, respectively. After 1 turn of HPT, there is a large fraction of green boundaries with misorientations of 5–15° while in the sample processed by 2 turns almost all boundaries are blue having misorientations between 15 and 60°. At the same time, the average area delineated by the green and blue boundaries in Fig. 6a (after 1 turn) is similar to the average area bounded by the blue boundaries in Fig. 6b (after 2 turns). This observation suggests that the boundaries with misorientations of 5–15° transform into HAGBs having misorientations between 15 and 60° when the number of turns increases from 1 to 2.

Table 3
The parameters of the microstructure obtained by EBSD and XLPA. $< x >_{area}$ is the area-weighted mean crystallite size and ρ is the dislocation density. The fractions of LAGBs and HAGBs are also listed.

Sample	Location	EBSD results			XLPA results	
		Grain size [μm]	Fraction of LAGBs [%]	Fraction of HAGBs [%]	$< x >_{area}$ [nm]	ρ [10^{14} m^{-2}]
N=1	center	3.3 ± 0.3	64	36	153 ± 15	1.8 ± 0.3
	half-radius	1.4 ± 0.1	45	55	96 ± 10	2.3 ± 0.3
	periphery	0.63 ± 0.06	46	54	93 ± 10	3.5 ± 0.5
N=2	center	1.9 ± 0.2	56	44	121 ± 13	1.5 ± 0.3
	half-radius	0.64 ± 0.06	40	60	115 ± 12	3.1 ± 0.5
	periphery	0.44 ± 0.05	46	54	89 ± 10	4.7 ± 0.7
N=4	center	1.9 ± 0.2	58	42	116 ± 12	1.4 ± 0.3
	half-radius	0.59 ± 0.06	38	62	92 ± 9	6.0 ± 0.5
	periphery	0.41 ± 0.04	27	73	77 ± 8	6.8 ± 0.7

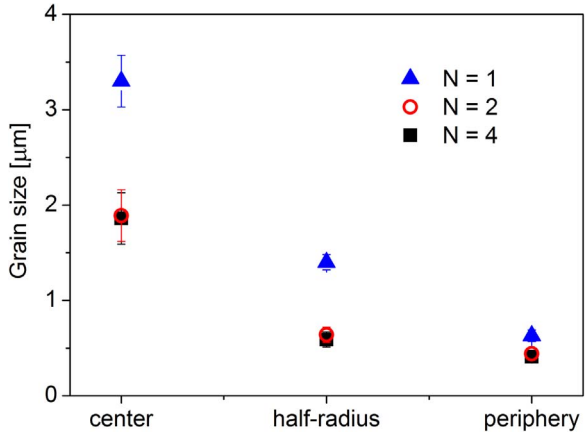

Fig. 5. The grain size for the center, half-radius and periphery of the disks processed by HPT for 1, 2 and 4 turns.

The crystallite size, the dislocation density and the twin fault probability of the samples were investigated by XLPA. As an example, Fig. 7 shows the CMWP fitting for the periphery of the sample processed by 4 revolutions of HPT. The mean crystallite size and the dislocation density for the center, half-radius and periphery of the disks processed by different numbers of turns are listed in Table 3. The twin fault probability was under the detection limit of the present XLPA method for all samples, which indicates that significant twinning did not occur during the consolidation of the aluminum powder by HPT.

The dislocation density in the disk center for all turns is 1.4–1.8×10^{14} m^{-2}. At the half-radius and periphery of the disks, the high shear strains yielded a significant increase in the dislocation density and a slight reduction of the crystallite size. Fig. 8a shows the dislocation density for the center, half-radius and periphery of the disks processed by HPT for 1, 2 and 4 turns. It can be seen that the dislocation density considerably increases with increasing the distance from the disk center for all numbers of turns and also with increasing the number of turns at both the half-radius and the periphery. Fig. 8b shows the dislocation density as a function of the shear strain calculated as $2\pi Nr/l$, where l is the height of the disk. The dislocation density increases monotonously with increasing the shear strain and saturates at the value of 6.8 ± 0.7×10^{14} m^{-2}.

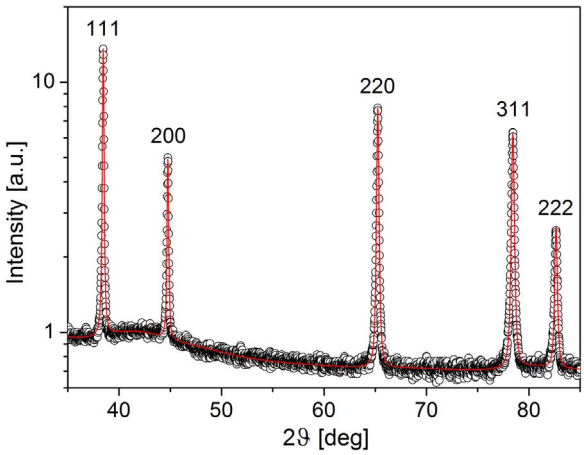

Fig. 7. A part of the X-ray diffraction pattern obtained at the periphery of the sample processed by 4 turns of HPT. The open circles and the solid line represent the measured data and the fitted pattern obtained by CMWP method, respectively. The intensity is in logarithmic scale.

3.2. Mechanical characterization of the consolidated aluminum samples

Fig. 9 shows two-dimensional hardness maps for N=1, 2 and 4 turns of HPT. The hardness increases with increasing both the distance from the center and the number of turns. For higher number of revolutions, the area of the soft center part shrinks. The maximum hardness value measured at the periphery of the disks processed by 4 turns is about 135 HV. Fig. 9 also reveals a variation of the hardness in the axial direction (i.e., perpendicular to the disk surface).

Representative engineering stress-strain curves obtained by tension on the specimens manufactured from the half-radius of the disks processed by HPT for N=1, 2 and 4 revolutions, are shown in Fig. 10. The yield strength at the half-radius for each HPT turn was determined as the average of the values obtained for the different specimens fabricated from the same disk. The yield strength for N=1, 2 and 4 turns are listed in Table 4. It can be seen that the yield strength increases from 163 ± 14 to 195 ± 10 MPa, when the number of turns increases from 1 to 4. The average ultimate tensile strength (UTS) and elongation to failure values are also given in Table 4. Already after 1 turn of HPT the UTS has a value of 290 ± 13 MPa which increased to 373 ± 23 MPa after 4 revolutions. In addition to the high strength values, the present HPT-consolidated aluminum samples exhibit large

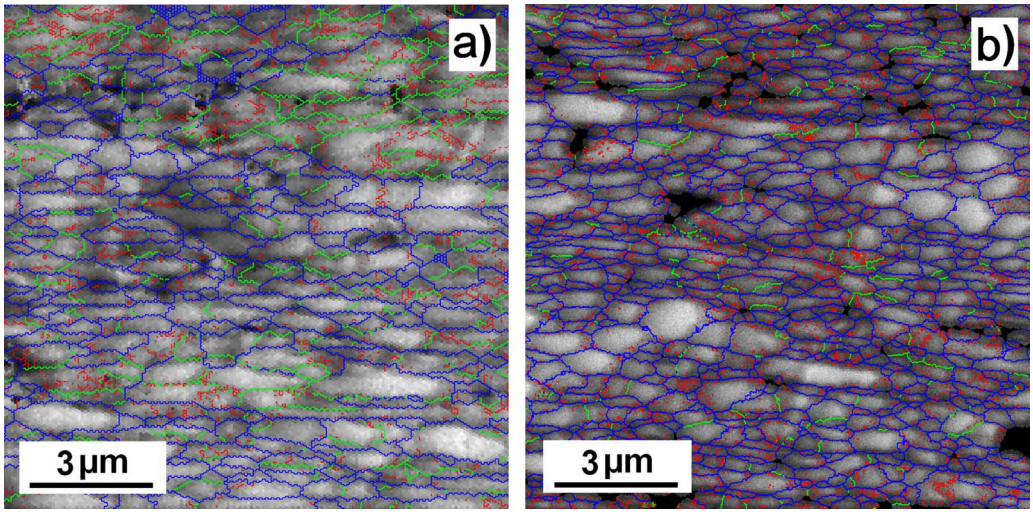

Fig. 6. Combined IQ and grain boundary maps for the half-radii of the samples processed by (a) 1 and (b) 2 turns of HPT. Red, green and blue colors indicate misorientations in the ranges of 2–5°, 5–15° and 15–60°, respectively. (For interpretation of the references to color in this figure legend, the reader is referred to the web version of this article.)

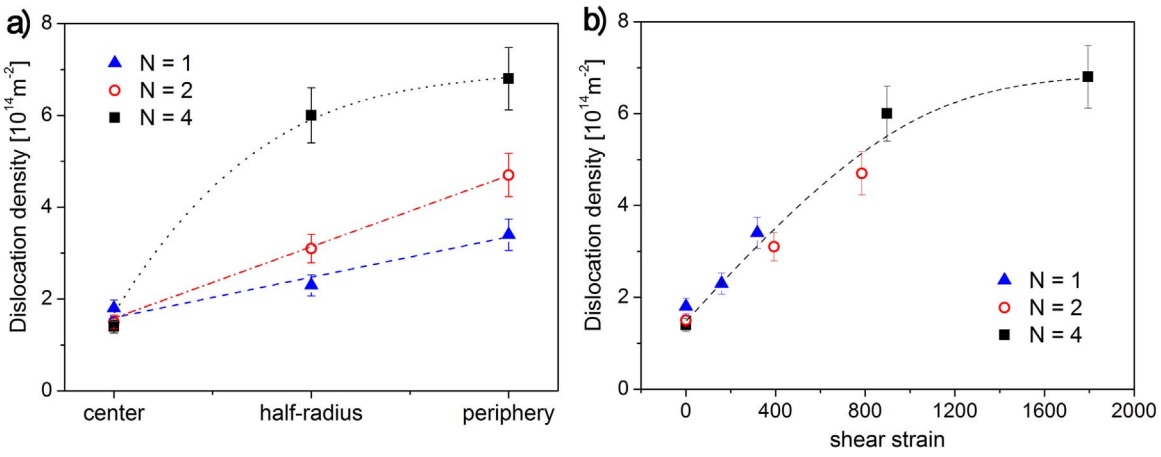

Fig. 8. (a) The dislocation density measured at the center, half-radius and periphery of the disks processed by HPT for 1, 2 and 4 turns. (b) The dislocation density values in (a) versus the shear strain of HPT processing.

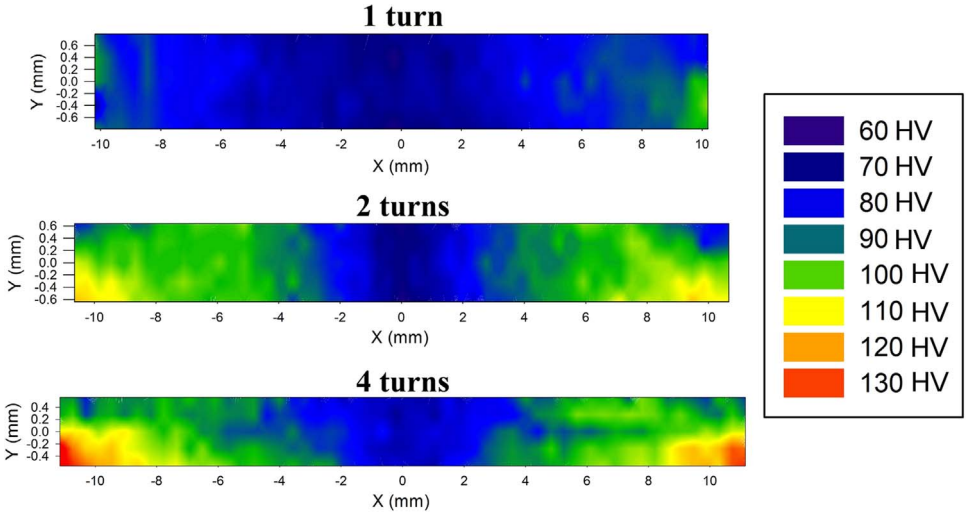

Fig. 9. Two-dimensional Vickers microhardness map measured on the cross section of the HPT-processed disks for N=1, 2 and 4 turns. The larger distance values at the disk periphery for the higher numbers of turns is caused by the extension of the samples in radial direction due to the semi-constrained HPT conditions.

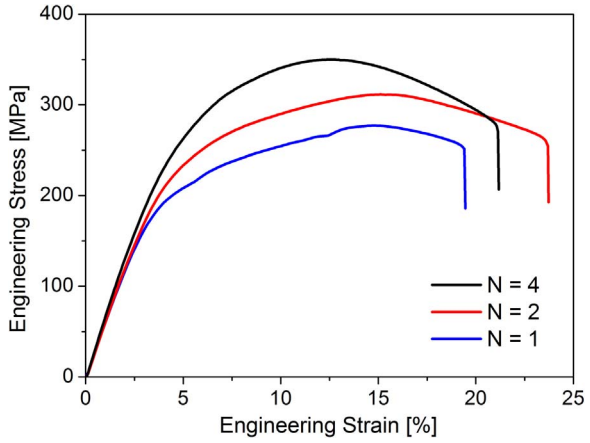

Fig. 10. Engineering stress-strain curves for pure aluminum samples consolidated by 1, 2 and 4 revolutions of HPT.

elongation to failure. The maximum achievable elongation after 1 turn is 18 ± 2%, which increases to 22–25% for the specimens processed by 2–4 revolutions of HPT. Moreover, the uniform elongation is also high as their values are between 12% and 15% for the samples processed by 1–4 turns.

4. Discussion

Table 3 shows that the crystallite size obtained by XLPA is about one order of magnitude smaller than the grain size determined by EBSD. The crystallite size (or coherently scattering domain size) determined by XLPA often differs from the grain size obtained by SEM, EBSD or transmission electron microscopy (TEM) [39–41]. Usually, the crystallite size determined by XLPA is equal or smaller than the grain size determined by microscopic methods. For SPD processed bulk metals and alloys, the grain size is 2–10 times larger than the crystallite size. This phenomenon can be attributed to the fact that the crystallites are equivalent to the domains in the microstructure which scatter X-rays coherently. As the coherency of X-rays breaks even if they are scattered from volumes having quite small misorientations (1–2°), the crystallite size corresponds rather to the subgrain size in severely deformed microstructures [42]. The LAGBs of subgrains often consist of dislocations with the same sign. It is noted that the detection limit of misorientation in EBSD is usually about 2°, therefore the subgrain boundaries with misorientations lower than 2° cannot be seen in the EBSD images. In addition to LAGBs, dipolar dislocation walls resulting in zero misorientation between the separated regions (cells) can also break the coherency of X-ray scattering [42]. These walls do not cause tilt or twist between the separated cells, however, the lattice planes in these cells are shifted relative to each other [42]. This shift varies randomly from cell to cell between 0 and $b/2$, where b is the

Table 4
The measured yield strength (σ_Y), ultimate tensile strength (UTS) and elongation to failure for the samples consolidated from 99.5% purity Al powder by HPT technique at room temperature. The data were taken from this study and the literature.

Reference	Starting material	conditions	σ_Y [MPa]	UTS [MPa]	Elongation to failure [%]
Present study	99.5% purity Al powder (~40 μm)	1.2 GPa, 1 turn, at half-radius	163 ± 14	290 ± 13	18 ± 2
		1.2 GPa, 2 turns, at half-radius	181 ± 5	344 ± 30	25 ± 2
		1.2 GPa, 4 turns, at half-radius	195 ± 10	373 ± 23	22 ± 1
Asgharzadeh et al.[35]	99.5% purity Al powder	6 GPa, 15 turns	210	296	23

magnitude of Burgers vector of dislocations. The shifts of the lattice planes yield uncorrelated phase shifts in the X-rays scattered by the different cells. This means that there is no coherency between the X-rays scattered by the volumes separated by the dipolar walls, and the line broadening is determined by the average cell size instead of the larger grain size [42]. As a consequence, the crystallite size obtained by XLPA corresponds to the size of subgrains or dislocation cells in the materials where these boundaries exist. For metallic materials processed in either bulk or powder form without the application of severe plastic deformation (e.g., by condensation or deposition methods) the crystallite size obtained by XLPA agrees well with the grain or particle size determined by TEM, due to the lack of subgrain/dislocation cell structure.

Fig. 10 shows that the consolidated Al samples exhibit a combination of high strength and good ductility. The yield strength (σ_Y) can be related to the grain size (d) using the Hall-Petch equation:

$$\sigma_Y=\sigma_0^{HP}+k_y d^{-1/2}, \quad (4)$$

where σ_0^{HP} is a thresold stress (often referred to as friction stress) and k_y is the Hall-Petch slope. The measured yield strength versus $d^{-1/2}$ is plotted in Fig. 11. A linear fitting on the datum points yields ~111 MPa and ~60 MPa $\mu m^{1/2}$ for σ_0^{HP} and k_y, respectively. The Hall-Petch slope obtained for the present consolidated Al materials is in a reasonable agreement with the value ofk_y (~63 MPa $\mu m^{1/2}$) determined for bulk UFG Al1050 alloy [43] which has similar chemical composition as that for the present material determined by OES analysis. At the same time, the friction stress for the consolidated samples (~111 MPa) is considerably larger than the value of σ_0^{HP} for the bulk UFG Al1050 alloy (~60 MPa). This difference can be explained by the light element content (such as oxygen) of the present material which cannot be measured by OES method. Indeed, energy-dispersive X-ray spectroscopy (EDS) in SEM revealed 2–3 at% oxygen in the consolidated aluminum samples. Most probably, this oxygen can be found in oxide/hydroxide dispersoids, which are usually unavoidable in powder metallurgy. This oxide or hydroxide phase forms from the native layer on the surfaces of the initial Al powder particles. Former studies (e.g.

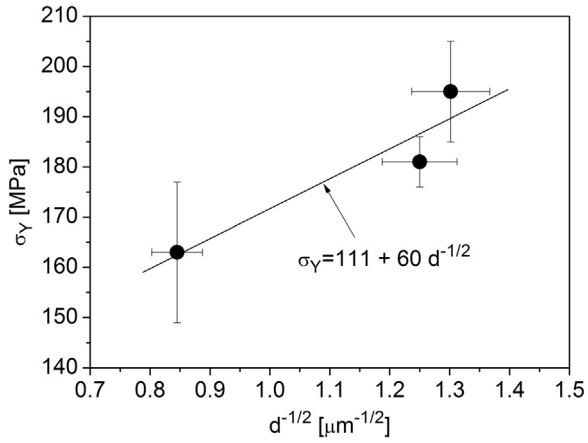

Fig. 11. The measured yield strength (σ_Y) versus the inverse square root of the grain size ($d^{-1/2}$) for the samples consolidated by 1, 2 and 4 turns of HPT. The straight line was fitted according to the Hall-Petch equation.

[44],) haveshown that the oxide/hydroxide layer on the surface of metallic particles with the size of several tens of microns may be as thick as 50 nm. During HPT processing these surface layers are fragmented into dispersoids and they are embedded in the Al matrix. Most probably, such an oxide/hydroxide phase is the source of oxygen detected by EDS. It should be noted that although crystalline oxide or hydroxide phase in the present Al samples was not observed by X-ray diffraction, its existence cannot be excluded, as demonstrated in a previous experiment [45]. Iftheoxide/hydroxide dispersoids have low fraction and small size, their diffraction peaks are broad and have low maxima, therefore they cannot be distinguished from the background. In addition, the surface native layer may be amorphous [46], andinthis case diffraction peaks from the secondary phase cannot be observed. Both solid solution and dispersion strengthening effects caused by the metallic impurities and the oxide/hydroxide particles are incorporated in the friction stress, resulting in its relatively high value.

In the present Al consolidated by HPT, the maximum dislocation density achieved after 4 turns was 6.8×10^{14} m^{-2}. Former studies [47–49] have shown that the saturation value of the dislocation density in bulk Al samples processed by SPD at room temperature strongly depends on the alloying element concentration. For 4N purity Al, Al-1%Mg and Al-3%Mg processed by equal channel angular pressing (ECAP), the maximum achievable dislocation density values were 1.8, 3.9 and 23×10^{14} m^{-2}, respectively. The higher alloying element concentration yielded larger saturation dislocation density due to the hindering effect of solute atoms on annihilation of dislocations during ECAP. HPT resulted similar maximum dislocation densities for these alloys as EACP processing [50]. The dislocation density for the 2N5 purity Al alloy studied in this paper is between the values obtained for Al-1%Mg and Al-3%Mg alloys. This means that there must be an additional hindering effect on dislocation annihilation in addition to the influence of the 0.5% metallic impurities in our samples. This additional effect may be caused by the oxide/hydroxide phase, as discussed in the previous paragraph.

Fig. 8 demonstrates that the three samples consolidated by 1, 2 and 4 turns exhibit large strain hardening in the beginning of tension. This behavior most probably has an important contribution to the relatively high values of uniform elongation (12–15%), in accordance with the Considére criterion [51]. Moreover, the total elongation has also high values (about 20%). Similar good ductility values have been reported in the literature for another 99.5% purity Al sample consolidated by HPT [35], as shown in Table 4. It should be noted that the fragmentation of the native surface layers during consolidation is beneficial to the ductility of the samples as the bonding between the freshly created Al particle surfaces without oxide/hydroxide layers is stronger. The present study demonstrates the capability of HPT to consolidate Al samples exhibiting high hardness and good ductility. The high strength of the Al samples consolidated in this work can be attributed to (i) the small grain size, (ii) the fine oxide/hydroxide dispersoids formed by fragmentation of the native surface layer and (iii) the nearly full densification (see Table 2) achieved by HPT. The latter effect can be attributed to the semi-constrained condition of HPT and the deformable powder holder, which allow a radial flow of the powder material during consolidation. This process might facilitate pore closing during HPT, resulting in samples with high density, good ductility and large

strength.

5. Conclusions

The microstructure and the mechanical performance of UFG aluminum consolidated by HPT were investigated. The numbers of HPT turns were 1, 2 and 4. The following results were obtained:

1. A high relative density was achieved already after 1 turn of HPT which slightly increased with increasing number of revolutions and reached 99.83% after 4 turns. The size of the particles in the initial powder was between 5 and 40 μm. In the HPT-processed samples, the grain size decreased with increasing both the distance from the disk center and the number of turns. However, between 2 and 4 turns further grain refinement was not observed. The smallest grain size with the value of 0.41 μm was achieved at the periphery of the disks processed for 2 and 4 turns. The fraction of HAGBs increases with increasing the distance from the disk center, however considerable difference between the HAGB fractions determined at the half-radius and the periphery was not observed. The highest fraction of HAGBs was achieved at the periphery of the disk processed by 4 revolutions (~73%).
2. The dislocation density increased with increasing both the distance from the disk center and the number of HPT turns. The dislocation density is a monotonously increasing function of the shear strain applied in HPT processing. The maximum dislocation density was 6.8×10^{14} m^{-2} which was achieved at the periphery of the sample processed by 4 turns.
3. The hardness increases with increasing both the number of turns and the distance from the center even after 4 turns. The maximum hardness value measured at the periphery of the disks processed by 4 turns was about 135 HV. Two-dimensional hardness maps measured on the cross-section of the disks revealed a hardness inhomogeneity in the axial direction.
4. The yield strength at the half-radius of the disks obtained by tension increased with increasing number of turns and achieved a maximum value of ~195 MPa. The yield strength versus grain size relationship obeys the Hall-Petch equation with a similar slope as determined for bulk UFG Al1050 with a similar impurity content. At the same time, the friction stress for the consolidated Al was higher than that for the bulk counterpart, most probably due to the oxide/hydroxide phase formed from the native layer on the powder particle surfaces. The sample consolidated by 4 turns of HPT exhibited a high ultimate tensile strength of ~373 MPa and a large elongation to failure of ~22%. The good tensile ductility is most probably caused by the enhanced strain hardening ability and the low porosity of the samples.

Acknowledgement

This work was financially supported partly by the Hungarian Scientific Research Fund, OTKA, Grant nos. K-109021 and PD-121049, and partly by Shiraz University under the Grant No. of Eng. 94GRD1M1818. Some of the authors (M.K.N, M.H.P and R.E) thank Mr. S.M. Arab and Mr. M. Shamsi for their kind assistance during this project. The authors are obliged to Mr. Gábor Varga for EBSD investigations.

References

[1] T.G. Langdon, Acta Mater. 61 (2013) 7035–7059.
[2] A. Azushima, R. Kopp, A. Korhonen, D. Yang, F. Micari, G. Lahoti, P. Groche, J. Yanagimoto, N. Tsuji, A. Rosochowski, CIRP Ann. Manuf. Technol. 57 (2008) 716–735.
[3] A. Mashreghi, L. Ghalandari, M. Reihanian, M. Moshksar, Mater. Sci. Forum, Trans. Tech. Publ. (2010) 131–150.
[4] R. Valiev, Nat. Mater. 3 (2004) 511–516.
[5] A.P. Zhilyaev, T.G. Langdon, Prog. Mater. Sci. 53 (2008) 893–979.
[6] A. Zhilyaev, G. Nurislamova, B.-K. Kim, M. Baró, J. Szpunar, T. Langdon, Acta Mater. 51 (2003) 753–765.
[7] K. Edalati, Z. Horita, Mater. Sci. Eng. A 652 (2016) 325–352.
[8] K. Edalati, Z. Horita, Mater. Sci. Eng. A 528 (2011) 7514–7523.
[9] A. Zhilyaev, T. McNelley, T. Langdon, J. Mater. Sci. 42 (2007) 1517–1528.
[10] K. Edalati, M. Ashida, Z. Horita, T. Matsui, H. Kato, Wear 310 (2014) 83–89.
[11] H. Bahmanpour, Y. Sun, T. Hu, D. Zhang, J. Wongsa-Ngam, T.G. Langdon, E.J. Lavernia, J. Mater. Res. 29 (2014) 578–585.
[12] C. Borchers, C. Garve, M. Tiegel, M. Deutges, A. Herz, K. Edalati, R. Pippan, Z. Horita, R. Kirchheim, Acta Mater. 97 (2015) 207–215.
[13] J.M. Cubero-Sesin, Z. Horita, Mater. Sci. Eng. A 558 (2012) 462–471.
[14] K. Edalati, Z. Horita, Scr. Mater. 63 (2010) 174–177.
[15] K. Edalati, S. Toh, Y. Ikoma, Z. Horita, Scr. Mater. 65 (2011) 974–977.
[16] K. Edalati, M. Arimura, Y. Ikoma, T. Daio, M. Miyata, D.J. Smith, Z. Horita, Mater. Res. Lett. 3 (2015) 216–221.
[17] S. Sabbaghianrad, T.G. Langdon, Mater. Sci. Eng. A 655 (2016) 36–43.
[18] Y. Xue, B. Jiang, L. Bourgeois, P. Dai, M. Mitome, C. Zhang, M. Yamaguchi, A. Matveev, C. Tang, Y. Bando, Mater. Des. 88 (2015) 451–460.
[19] P. Jenei, E.Y. Yoon, J. Gubicza, H.S. Kim, J.L. Lábár, T. Ungár, Mater. Sci. Eng. A 528 (2011) 4690–4695.
[20] M. Jahedi, M.H. Paydar, M. Knezevic, Mater. Charact. 104 (2015) 92–100.
[21] M. Jahedi, M. Knezevic, M.H. Paydar, J. Mater. Eng. Perform. 24 (2015) 1471–1482.
[22] M. Jahedi, M.H. Paydar, S. Zheng, I.J. Beyerlein, M. Knezevic, Mater. Sci. Eng. A 611 (2014) 29–36.
[23] S.-H. Joo, H.S. Kim, Metall. Mater. Trans. A (2016).
[24] P. Pereira, R. Figueiredo, P. Cetlin, T. Langdon, IOP Conference Series: Materials Science and Engineering, IOP Publishing, Bristol, United Kingdom, 2014, p. 012041.
[25] B. Martin, S. Frantisek, B. Otto, G. Requena, Mater. Sci. Eng. A 504 (2009) 1–7.
[26] M. Paydar, M. Reihanian, E. Bagherpour, M. Sharifzadeh, M. Zarinejad, T. Dean, Mater. Des. 30 (2009) 429–432.
[27] X. Wei, B. Vekshin, V. Kraposhin, Y. Huang, J. Shen, K. Xia, Mater. Sci. Eng. A 528 (2011) 5784–5789.
[28] M. Jahedi, M.H. Paydar, Mater. Sci. Eng. A 527 (2010) 5273–5279.
[29] X. Wu, W. Xu, K. Xia, Mater. Sci. Eng. A 493 (2008) 241–245.
[30] K. Xia, Adv. Eng. Mater. 12 (2010) 724–729.
[31] M. Balog, C. Poletti, F. Simancik, M. Walcher, W. Rajner, J. Alloy. Compd. 509 (2011) S235–S238.
[32] A. Bachmaier, R. Pippan, Mater. Sci. Eng. A 528 (2011) 7589–7595.
[33] C. Poletti, M. Balog, F. Simancik, H. Degischer, Acta Mater. 58 (2010) 3781–3789.
[34] H. Asgharzadeh, S.-H. Joo, H.S. Kim, Metall. Mater. Trans. A 46 (2015) 1838–1842.
[35] H. Asgharzadeh, S.-H. Joo, H.S. Kim, Metall. Mater. Trans. A 45 (2014) 4129–4137.
[36] L. Zhao, H. Lu, Z. Gao, Adv. Eng. Mater. 17 (2015) 976–981.
[37] S.-H. Joo, S.C. Yoon, C.S. Lee, D.H. Nam, S.H. Hong, H.S. Kim, J. Mater. Sci. 45 (2010) 4652–4658.
[38] G. Ribárik, J. Gubicza, T. Ungár, Mater. Sci. Eng. A 387 (2004) 343–347.
[39] T. Ungár, J. Gubicza, G. Ribárik, A. Borbély, J. Appl. Cryst. 34 (2001) 298–310.
[40] Y.T. Zhu, J.Y. Huang, J. Gubicza, T. Ungár, Y.M. Wang, E. Ma, R.Z. Valiev, J. Mat. Res. 18 (2003) 1908–1917.
[41] M. Samadi Khoshkhoo, J. Scudino, S., T. Thomas, H. Wendrock Gemming, J. Eckert, Mater. Lett. 108 (2013) 343–345.
[42] T. Ungár, G. Tichy, J. Gubicza, R.J. Hellmig, Powder Diffr. 20 (2005) 366–375.
[43] Y.S. Sato, M. Urata, H. Kokawa, K. Ikeda, Mater. Sci. Eng. A 354 (2003) 298–305.
[44] E.Y. Yoon, D.J. Lee, T.-S. Kim, H.J. Chae, P. Jenei, J. Gubicza, T. Ungár, M. Janecek, J. Vratna, S.H. Lee, H.S. Kim, J. Mater. Sci. 47 (2012) 7117–7123.
[45] H. Li, A. Misra, Y. Zhu, Z. Horita, C.C. Koch, T.G. Tokunaga, Mater. Sci. Eng. A 523 (2009) 60–64.
[46] G. Dirras, J. Gubicza, D. Tingaud, S. Billard, Mater. Chem. Phys. 129 (2011) 846–852.
[47] J. Gubicza, N.Q. Chinh, Z. Horita, T.G. Langdon, Mater. Sci. Eng. A 387–389 (2004) 55–59.
[48] J. Gubicza, N.Q. Chinh, Gy Krállics, I. Schiller, T. Ungár, Curr. Appl. Phys. 6 (2006) 194–199.
[49] O. Andreau, J. Gubicza, N.X. Zhang, Y. Huang, P. Jenei, T.G. Langdon, Mater. Sci. Eng. A 615 (2014) 231–239.
[50] J. Gubicza, Defect Structure In Nanomaterials, Woodhead Publishing Ltd, Cambridge, UK, 2012.
[51] I.S. Yasnikov, A. Vinogradov, Y. Estrin, Scr. Mater. 76 (2014) 37–40.